Hindawi Publishing Corporation
Journal of Drug Delivery
Volume 2011, Article ID 203986, 7 pages
doi:10.1155/2011/203986

Research Article

Local Gene Delivery System by Bubble Liposomes and Ultrasound Exposure into Joint Synovium

Yoichi Negishi,[1] Yuka Tsunoda,[1] Yoko Endo-Takahashi,[1] Yusuke Oda,[2] Ryo Suzuki,[2] Kazuo Maruyama,[2] Matsuo Yamamoto,[3] and Yukihiko Aramaki[1]

[1] *Department of Drug and Gene Delivery Systems, School of Pharmacy, Tokyo University of Pharmacy and Life Sciences, 1432-1 Horinouchi, Hachioji, Tokyo 192-0392, Japan*
[2] *Department of Biopharmaceutics, Teikyo University, 1091-1 Suwarashi, Midori-ku, Sagamihara, Kanagawa 252-5195, Japan*
[3] *Department of Periodontology, Showa University School of Dentistry, 2-1-1 Kitasenzoku, Ohta-ku, Tokyo 145-8515, Japan*

Correspondence should be addressed to Yoichi Negishi, negishi@toyaku.ac.jp

Received 17 January 2011; Accepted 1 March 2011

Academic Editor: Susan Hua

Recently, we have developed novel polyethylene glycol modified liposomes (bubble liposomes; BL) entrapping an ultrasound (US) imaging gas, which can work as a gene delivery tool with US exposure. In this study, we investigated the usefulness of US-mediated gene transfer systems with BL into synoviocytes *in vitro* and joint synovium *in vivo*. Highly efficient gene transfer could be achieved in the cultured primary synoviocytes transfected with the combination of BL and US exposure, compared to treatment with plasmid DNA (pDNA) alone, pDNA plus BL, or pDNA plus US. When BL was injected into the knee joints of mice, and US exposure was applied transcutaneously to the injection site, highly efficient gene expression could be observed in the knee joint transfected with the combination of BL and US exposure, compared to treatment with pDNA alone, pDNA plus BL, or pDNA plus US. The localized and prolonged gene expression was also shown by an *in vivo* luciferase imaging system. Thus, this local gene delivery system into joint synovium using the combination of BL and US exposure may be an effective means for gene therapy in joint disorders.

1. Introduction

Intra-articular gene therapy is considered a feasible technique to deliver therapeutic proteins to suppress inflammation and destruction of the joints in rheumatoid arthritis and osteoarthritis, because it could minimize extra-articular adverse effects linked to the systemic injection of drugs [1, 2]. To achieve successful gene therapy in a clinical setting, it is critical that the gene delivery system is safe, easy to apply, and provides therapeutic transgene expression. Previous studies using viral vectors reported the successful transfer of therapeutic genes into the target cells in joint diseases [1, 2], but because of the considerable immunogenicity related to the use of viruses, nonviral gene transfer still needs to be developed [3]. Recently, it has been reported that therapeutic ultrasound as a physical non-viral gene transfer method enables genes to permeate cell membranes. Acoustic cavitation is involved in the mechanism of gene transfer [4–8]; however, to achieve efficient gene transfer, high intensity ultrasound (US) is needed, leading to tissue damage [9–11]. In contrast, low-intensity US in combination with microbubbles has recently acquired much attention as a safe method of gene delivery [12–16]; however, microbubbles have problems with size, stability, and targeting function. Liposomes have been known as drug, antigen, and gene delivery carriers [17–21]. To solve the above-mentioned issues of microbubbles, we previously developed polyethylene glycol- (PEG-) modified liposomes entrapping echo contrast, bubble liposomes (BL), which can function as a novel gene delivery tool by applying them with US exposure [22–27].

The establishment of a method to deliver genes into joints by the combination of BL and US exposure may facilitate the development of a safe and efficient gene therapy for joint disorders. In the present study, we investigated the usefulness of US-mediated gene transfer systems with BL into synoviocytes *in vitro* and the joint synovium *in vivo*.

2. Materials and Methods

2.1. Preparation of Bubble Liposomes. Bubble liposomes were prepared by the previously described methods [22, 23, 26]. Briefly, PEG liposomes composed of 1,2-dipalmitoyl-*sn*-glycero-3-phosphocholine (DPPC) (NOF Corporation, Tokyo, Japan) and 1,2-distearoyl-*sn*-glycero-3-phosphatidyl-ethanolamine-polyethylen eglycol (DSPE-PEG_{2000}-OMe) (NOF Corporation) in a molar ratio of 94 : 6 were prepared by a reverse phase evaporation method. In brief, the reagents were dissolved 1 : 1 (v/v) in chloroform/diisopropyl ether. Phosphate-buffered saline was added to the lipid solution, and the mixture was sonicated and then evaporated at 47°C. The organic solvent was completely removed, and the size of the liposomes was adjusted to less than 200 nm using extruding equipment and a sizing filter (pore size: 200 nm) (Nuclepore Track-Etch Membrane, Whatman plc, UK). The lipid concentration was measured using a Phospholipid C test Wako (Wako Pure Chemical Industries, Ltd., Osaka, Japan). BL were prepared from liposomes and perfluoropropane gas (Takachio Chemical Ind. Co. Ltd., Tokyo, Japan). First, 2 mL sterilized vials containing 0.8 mL liposome suspension (lipid concentration: 1 mg/mL) were filled with perfluoropropane gas, capped, and then pressurized with a further 3 mL perfluoropropane gas. The vial was placed in a bath-type sonicator (42 kHz, 100 W) (BRANSONIC 2510j-DTH; Branson Ultrasonics Co., Danbury, Conn, USA) for 5 min to form BL.

2.2. Plasmid DNA. The plasmid pCMV-Luc is an expression vector encoding the firefly luciferase gene under the control of a cytomegalovirus promoter. The plasmid pDsRed-Express-N1 (Clontech Laboratories, Inc., Mountain View, Calif, USA) is an expression vector encoding the red fluorescent protein under the control of a cytomegalovirus promoter.

2.3. Transfection of Plasmid DNA into Primary Synoviocytes Using Bubble Liposomes. Primary synoviocytes (HFLS), which are primary fibroblast-like cells derived from the inflamed synovial tissue of rheumatoid arthritis patients, were purchased from Cell Applications, Inc. (San Diego, Calif, USA). The culture was performed according to the manufacturer's instructions. The day before transfection, cells (3×10^4) were seeded in the wells of a 48-well plate (ASAHI TECHNOGLASS CO., Chiba, Japan). Five micrograms of pDNA and 60 μg BL were mixed together with culture medium containing 10% FBS and added to the cells. The cells were immediately exposed to US (frequency, 2 MHz, duty, 50%; burst rate, 2.0 Hz; intensity, 2.5 W/cm^2) for 10 sec through a 6-mm diameter probe placed in the well. A Sonopore 3000 (NEPA GENE, Co., Ltd., Chiba, Japan) was used to generate the US. The cells were washed twice with culture medium and cultured for two days. The cell lysate was prepared with lysis buffer (0.1 M Tris-HCl (pH 7.8), 0.1% Triton X-100, and 2 mM EDTA). Luciferase activity was measured using a luciferase assay system (Promega, Madison, WI) and a luminometer (LB96V; Belthold Japan Co. Ltd., Tokyo, Japan). The activity is indicated as relative light units (RLU) per mg of protein.

2.4. Transfection of Plasmid DNA with Lipofectamine 2000. The day before transfection, HFLS-RA (4×10^4) were seeded in the wells of a 48-well plate (ASAHI TECHNOGLASS CO., Chiba, Japan). Then, 0.25 μg pDNA (final concentration, 25 nM) wsa diluted in Opti-MEM (GIBCO). Next, 1.25 μg Lipofectamine 2000 (LF2000) (Invitrogen Japan K.K., Tokyo, Japan) was diluted in Opti-MEM. These solutions were mixed and added to the cells. After 4 and 24 hours, the cells were washed with PBS and cultured for two days. The experiments were performed according to the manufacturers' instructions.

2.5. Measurement of Luciferase and DsRed Expression. Cell lysate was prepared with lysis buffer (0.1 M Tris-HCl (pH 7.8), 0.1% Triton X-100, and 2 mM EDTA). Luciferase activity was measured using a luciferase assay system (Promega, Madison, WI) and a luminometer (LB96V; Belthold Japan Co. Ltd.). The activity is indicated as relative light units (RLU) per mg protein. To analyze DsRed expression, the treated cells were observed with a fluorescence microscope (Axiovert 200 M; Carl Zeiss).

2.6. In Vivo Gene Delivery into the Joint Synovium of Mice with Bubble Liposomes and Ultrasound Exposure. To determine the efficiency of gene delivery, animals were divided into five experimental groups and one control group ($n = 4$ in each group). ICR mice (5 weeks old, male) were anesthetized with an *i.p.* injection of sodium pentobarbital (80 mg/kg) throughout each procedure. A 40 μL suspension of pDNA (20 μg) and BL (30 μg) was injected into the knee joint of the ICR mice, and US exposure (frequency, 1 MHz; duty, 50%; intensity, 2 W/cm^2; time, 60 sec) was immediately applied at the injection site. Five days after the injection, the mice were euthanized and sacrificed, and the knee joint tissue in the US-exposed area was collected and homogenized. The tissue homogenates were prepared with lysis buffer (0.1 M Tris-HCl (pH 7.8), 0.1% Triton X-100, and 2 mM EDTA). Luciferase activity was measured using a luciferase assay system (Promega, Madison, WI) and a luminometer (LB96V; Belthold Japan Co. Ltd.). Activity is indicated as relative light units (RLU) per mg of protein.

2.7. In Vivo Luciferase Imaging. To determine the efficiency of gene delivery, animals were divided into five experimental groups and one control group ($n = 4$ in each group). ICR mice (5 weeks old, male) were anesthetized with an *i.p.* injection of sodium pentobarbital (80 mg/kg) throughout each procedure. A 40 μL suspension of pDNA (20 μg) and BL (30 μg) was injected into the knee joint of the ICR mice, and US exposure (frequency, 1 MHz; duty, 50%; intensity, 2 W/cm^2; time, 60 sec) was immediately applied at the injection site. Several days after the injection, the mice were anaesthetized and *i.p.* injected with D-luciferin (150 mg/kg) (Xenogen Corporation, Calif, USA). After 10 min, luciferase expression was observed with an *in vivo* luciferase imaging

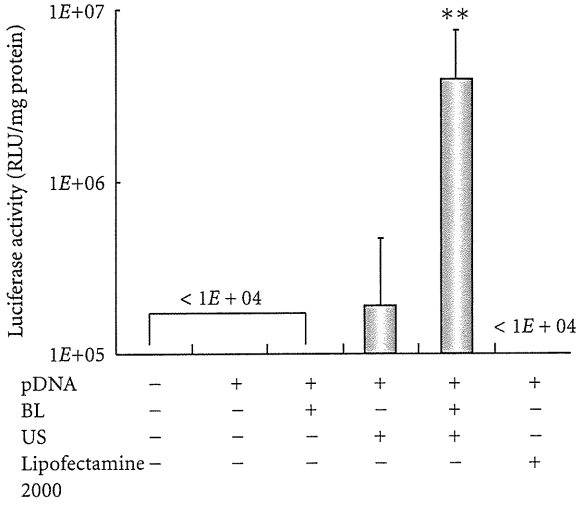

FIGURE 1: Luciferase expression in HFLS transfected with bubble liposomes and ultrasound exposure compared with Lipofectamine 2000. pDNA (pCMV-Luc) and BL were mixed together with culture medium and added to the HFLS. The cells were immediately exposed to US (frequency, 2 MHz; duty, 50%; intensity, 2.5 W/cm^2; US exposure time, 10 sec.). The cells were washed and cultured for 2 days, and then luciferase activity was determined as described in Section 2 . The transfection of pDNA by LF2000 was also performed according to the manufacturers' instructions. All data are shown as the mean ± SD ($n = 4$). $^{**}P < .05$ versus other treatment groups. BL: bubble liposomes; US: ultrasound exposure.

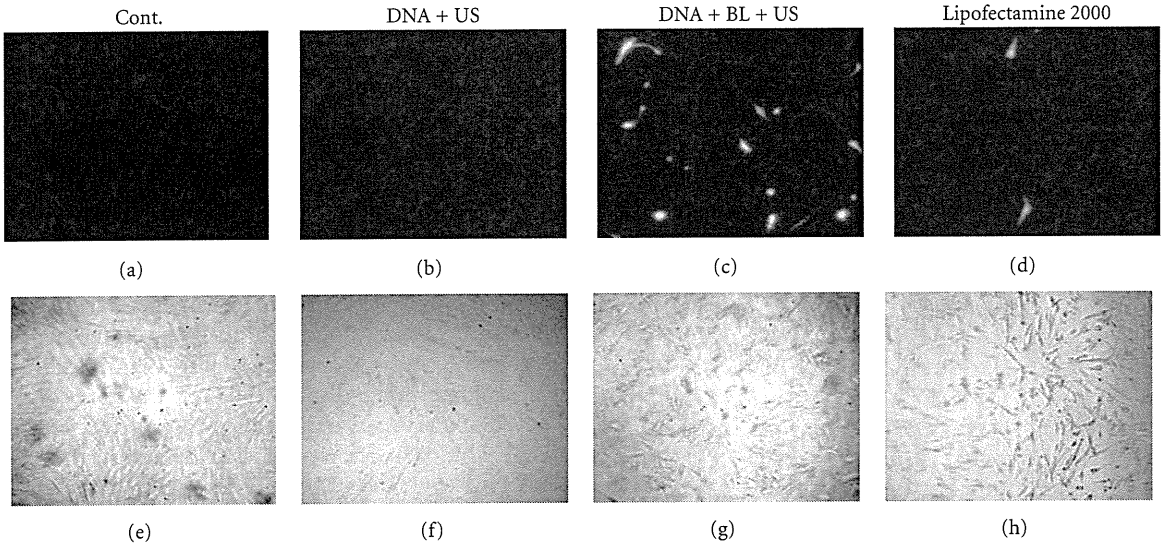

FIGURE 2: DsRed expression in HFLS transfected with bubble liposomes and ultrasound exposure compared with Lipofectamine 2000. pDNA (pDsRed-Express-N1) and BL were mixed together with culture medium and added to the HFLS. The cells were immediately exposed to US (frequency, 2 MHz; duty, 50%; intensity, 2.5 W/cm^2; US exposure time, 10 sec.). The cells were washed and cultured for 2 days and then treated cells were examined by a fluorescence microscope original magnification X200. Transfection of pDNA by LF2000 was also performed. BL: bubble liposomes; US: ultrasound exposure. Fluorescence, (a–d); phase contrast, (e–h).

system (IVIS) (Xenogen Corporation). The image of a representative of the 4 mice was used for each treatment group in this experiment.

2.8. Immunohistochemistry. The gene-transfected joint tissues were preserved in 10% PFA, decalcified with EDTA, and then embedded in paraffin and sectioned. Sections (3 μm thickness) were evaluated for the expression of luciferase protein by immunostaining. The sections were deparaffinized in xylene, rehydrated through graded ethanol, and equilibrated in PBS. The sections were incubated with biotin-labeled rabbit antiluciferase antibody (Cortex Biochem, San Leandro, Calif, USA). The following day, after three washes in PBS, immunoreactivity was detected using an antigoat IgG/HRP and diaminobenzidine (DAB). After color development, the joint sections were counterstained with hematoxylin and were then dehydrated, cleared, and mounted on slides.

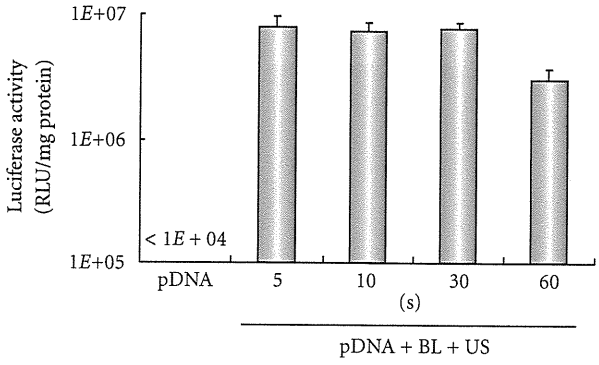

FIGURE 3: Effect of ultrasound exposure time on transfection with bubble liposomes into HFLS. pDNA (pCMV-Luc) and BL were mixed together with culture medium and added to the HFLS. The cells were immediately exposed to US (intensity, 2.5 W/cm^2; US exposure time, 5–60 sec.). The cells were washed and cultured for 2 days, and then luciferase activity was determined. All data are shown as the mean ± SD (n = 4). BL: bubble liposomes; US: ultrasound exposure.

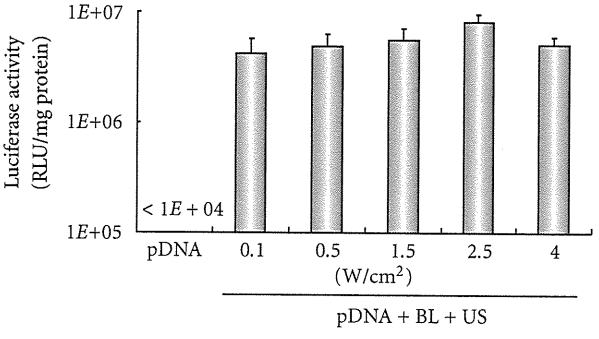

FIGURE 4: Effect of ultrasound intensity on transfection with Bubble liposomes into HFLS. pDNA (pCMV-Luc) and BL were mixed together with culture medium and added to the HFLS. The cells were immediately exposed to US (intensity, 0.1–4 W/cm^2; US exposure time, 10 sec.). The cells were washed and cultured for 2 days and then luciferase activity was determined. All data are shown as the mean ± SD (n = 4). BL: bubble liposomes; US: ultrasound exposure.

2.9. In Vivo Studies. Animal use and relevant experimental procedures were approved by Tokyo University of Pharmacy and Life Science Committee and Teikyo University on the Care and Use of Laboratory Animals. All experimental protocols for animal studies were in accordance with the Principle of Laboratory Animal Care at Teikyo University.

2.10. Statistical Analyses. All data are shown as the mean±SD (n = 4 or 6). Data were considered significant when $P < .05$. The t-test was used to calculate statistical significance.

3. Results and Discussion

3.1. Gene Transfection with Bubble Liposomes and Ultrasound Exposure into Synoviocytes In Vitro. It is known that microbubbles improve cell and tissue permeability by cavitation upon US exposure [11–15]. We first tried

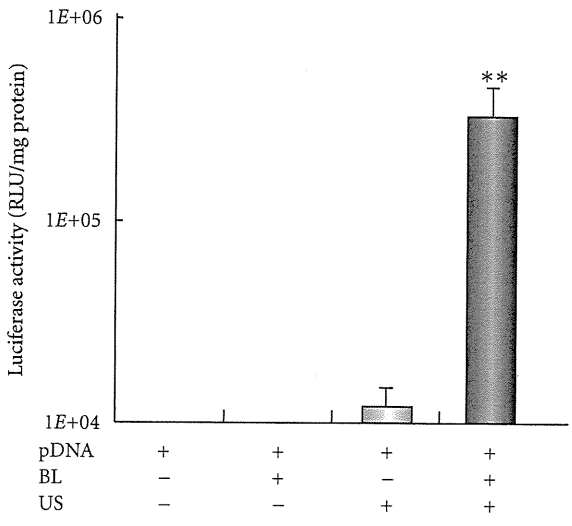

FIGURE 5: *In vivo* luciferase expression in the joint synovium after transfection with bubble liposome and ultrasound exposure. A suspension of pDNA and BL was injected into the knee joint of the mice, and US exposure (frequency, 1 MHz; duty, 50%; intensity, 2 W/cm^2; time, 60 sec) was immediately applied at the injection site. Five days after injection, the knee joint tissue in the US-exposed area was collected and homogenized. Luciferase activity was determined. All data are shown as the mean ± SD (n = 4). $^{**}P < .05$ versus other treatment groups. BL: bubble liposomes; US: ultrasound exposure.

to transfect naked pDNA (pCMV-Luc) into primary synoviocytes (HFLS), which are primary fibroblast-like cells derived from the inflamed synovial tissue of rheumatoid arthritis patients, by BL and/or US (Figure 1). As a result, luciferase activity in the group receiving a combination of BL with US exposure was 400- or 30-fold higher than that of the group treated with pDNA alone or pDNA plus US, respectively (Figure 1). For basic research, LF2000 is often used to transfect plasmid DNA or siRNA to analyze gene function in various cultured cell lines. We, therefore, compared with a commercially available transfection reagent, LF2000; however, luciferase activity was very low (Figure 1). Figure 2 shows the transfection efficiency using DsRed expressing plasmid DNA. The numbers of DsRed-positive cells markedly increased with the combination of BL and US exposure compared to the group treated with pDNA plus US or LF2000. It may be difficult to achieve efficient gene transfection to primary cultured cells by LF2000, because a low level of transfection efficiency in human umbilical vein endothelial cells (HUVEC) was also observed (data not shown). Our previous report showed that when the intracellular localization of fluorescent-labeled siRNA in COS7 cells just after transfection with BL and US exposure is examined by confocal laser scanning microscopy (CLSM) analysis, significant cytoplasmic distribution of siRNA can be observed [25]. Consequently, we concluded that unlike the transfection method with LF2000 involving endocytosis, transfection with BL and US does not involve endocytosis, but siRNA was directly and quickly introduced into the cytoplasm by physical force. Similarly, when fluorescent-labeled plasmid DNA was delivered to COS7 cells by the combination of BL and US exposure, plasmid DNA could

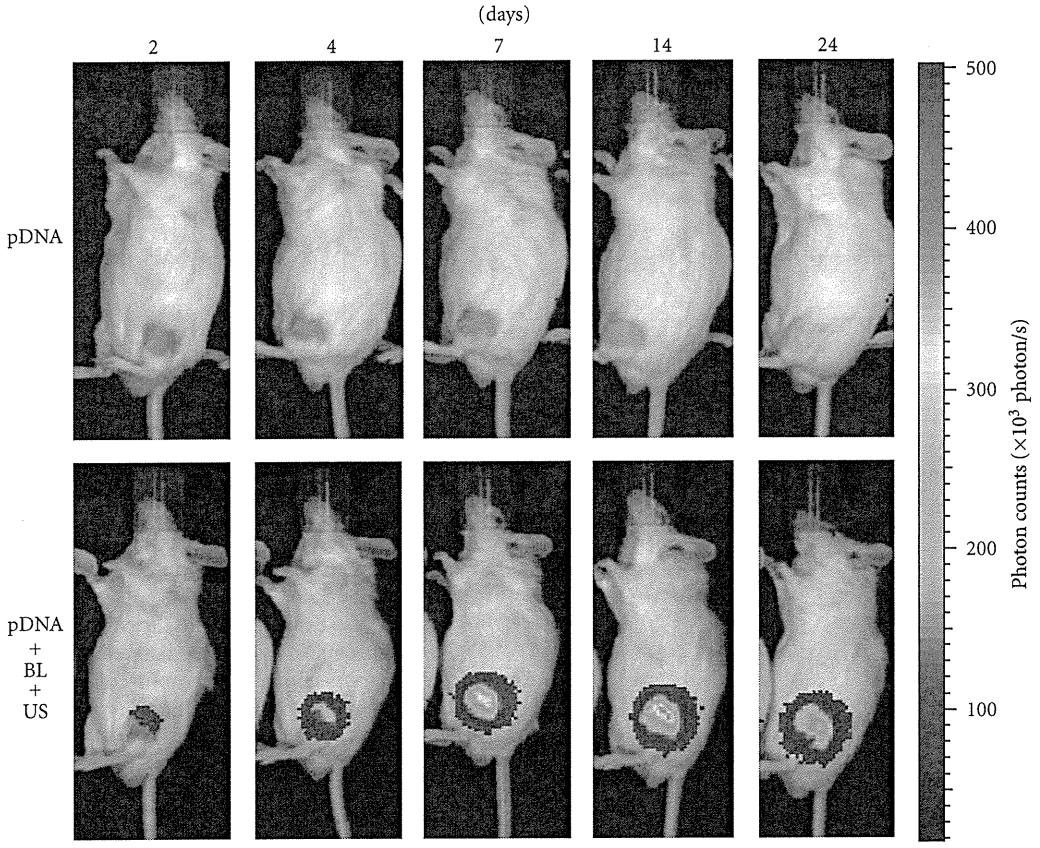

FIGURE 6: *In vivo* luciferase imaging. A suspension of pDNA and BL was injected into the knee joint of the mice, and US exposure (frequency, 1 MHz; duty, 50%; intensity, 2 W/cm^2; time, 60 sec) was immediately applied at the injection site. Luciferase expressions after transfection into the joint treated with pDNA, or pDNA plus BL plus US exposure were observed with an *in vivo* luciferase imaging system for 2–24 days.

be also distributed in the cytoplasm and nucleus (data not shown). Therefore, these results suggested that the combination of BL and US exposure facilitated the efficient transfection of pDNA into the cells due to the induction of cavitation.

Previously, our report demonstrated that gene transfection efficiency *in vitro* could be affected by increasing the US exposure time and intensity [22, 23]. We, therefore, examined the effect of US exposure time and intensity on transfection with BL into HFLS. High gene expression could be achieved by only 5 seconds of US exposure. In contrast, gene expression fell with a longer exposure time, 60 sec. (Figure 3), which might have been due to cytotoxicity. When we applied a range of US intensity (0.1–4 W/cm^2) in transfection, US intensity of 2.5 W/cm^2 was modestly higher than other treated groups (Figure 4). These results suggest that BL with US exposure is a useful gene delivery tool for *in vitro* transfection in synoviocytes.

3.2. Gene Transfection with Bubble Liposomes and Ultrasound Exposure into Joint Synovium In Vivo. A local gene delivery system to the joint synovium by BL and US exposure may be easily applied, because the injected BL may be retained in the confined joint space and percutaneous US exposure may induce cavitations on the surface of the synovium. We, therefore, attempted to deliver pCMV-Luc, luciferase-expressing plasmid DNA, into the joint synovium of mice using BL and US and to determine the level of the gene expression. A 40 μL solution of pDNA and BL was injected into the knee joint of the mice, and US exposure was immediately applied at the injection site. As a result, marked gene expression could be enhanced efficiently only with the combination of BL and US exposure when compared with other treatments (Figure 5). Exceeding our expectations, their gene expression was 500-fold higher than pDNA injection alone. We also observed luciferase gene expression area in the whole body using an *in vivo* luciferase imaging system during 2–24 days after transfection into a joint treated with pDNA, BL, and US exposure. The high level of gene expression persisted for 7–24 days after transfection using BL and US exposure (Figure 6). Gene expression was restricted to the area of US exposure. In contrast, no signal in the whole body was observed in the group with pDNA injection alone. This suggested that the combination of BL and US exposure facilitated the efficient transfection of pDNA into the joint tissue due to the induction of cavitation. We next investigated the localization of the transfected gene expression in the transfected joint by immunohistochemical analysis. This showed that the luciferase protein expression was limited to the synovial fibroblasts in the joint space. No

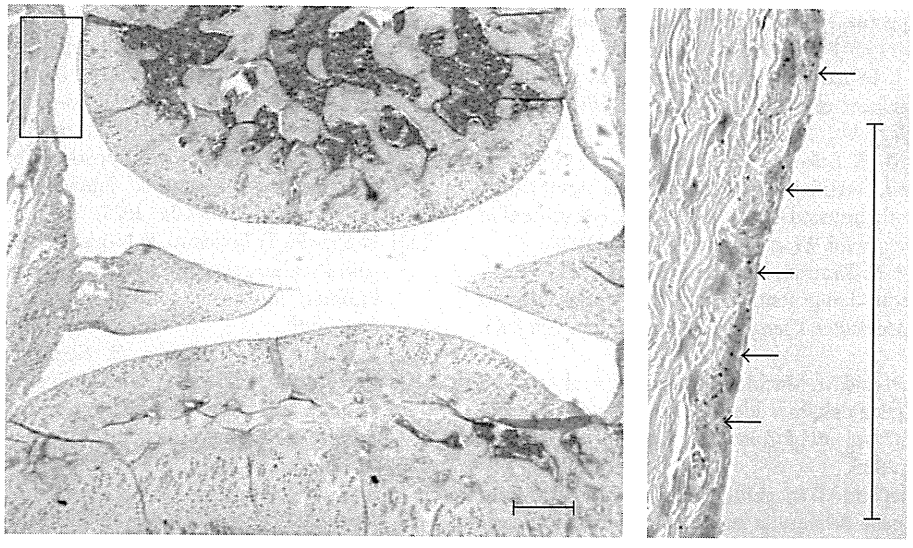

(a) (b)

FIGURE 7: Immunostaining for luciferase in synovial fibroblast. Local gene expression in joint synovium after intra-articular gene delivery using BL and US. Seven days after treatment, the expression of luciferase protein was mostly limited to the synovial fibroblasts. (a) H&E staining in joint sections. (b) Immunohistochemical localization of luciferase (arrows). Scale bar = 100 μm.

expression was observed in other tissues such as articular cartilage (Figure 7).

Gene transfer into cartilage may be difficult because cavitation induction with BL and US cannot reach chondrocytes embedded in extracellular matrix in articular cartilage, leading to no transfection. However, successful gene transfection into chondrocytes might be achieved by BL and US exposure, because articular chondrocytes in RA or OA are exposed by degradation of the extracellular matrix in articular cartilage in this stage of the disease.

It is known that cartilage degradation is the main pathological feature in OA; however, synovial factors are closely related to this progress [28], while synovitis is the main pathological feature of RA. Therefore, intra-articular gene therapy by BL and US exposure could be considered a feasible technique to deliver therapeutic proteins to suppress inflammation and destruction of the joints in RA and OA, because it could minimize extra-articular adverse effects linked to systemic injection of drugs; however, further study will be required for their assessment.

4. Conclusions

In this study, we showed that the combination of BL and US exposure could be an effective gene delivery method into synoviocytes *in vitro* and the joint synovium *in vivo*. In the future, this local gene delivery method with BL and US exposure might be used in non-viral gene therapy for joint disorders, such as RA and OA.

Acknowledgments

The authors are grateful to Dr. Katsuro Tachibana (Department of Anatomy, School of Medicine, Fukuoka University) for technical advice regarding the induction of cavitation with US and to Mr. Yasuhiko Hayakawa, Mr. Takahiro Yamauchi, and Mr. Kosho Suzuki (NEPA GENE CO., LTD.) for technical advice regarding US exposure. This study was supported in part by the Industrial Technology Research Grant Program (no. 04A05010) from New Energy, the Industrial Technology Development Organization (NEDO) of Japan, a Grant-in-Aid for Scientific Research (B) (no. 20300179) from the Japan Society of the Promotion of Science, and a grant for private universities provided by the Promotion and Mutual Aid Corporation for Private Schools of Japan. Y. Negishi and Y. Tsunoda contributed equally to this paper.

References

[1] C. H. Evans, P. D. Robbins, S. C. Ghivizzani et al., "Gene transfer to human joints: progress toward a gene therapy of arthritis," *Proceedings of the National Academy of Sciences of the United States of America*, vol. 102, no. 24, pp. 8698–8703, 2005.

[2] C. H. Evans, E. Gouze, J. N. Gouze, P. D. Robbins, and S. C. Ghivizzani, "Gene therapeutic approaches-transfer in vivo," *Advanced Drug Delivery Reviews*, vol. 58, no. 2, pp. 243–258, 2006.

[3] D. G. Miller, E. A. Rutledge, and D. W. Russell, "Chromosomal effects of adeno-associated virus vector integration," *Nature Genetics*, vol. 30, no. 2, pp. 147–148, 2002.

[4] M. Fechheimer, J. F. Boylan, S. Parker, J. E. Sisken, G. L. Patel, and S. G. Zimmer, "Transfection of mammalian cells with plasmid DNA by scrape loading and sonication loading," *Proceedings of the National Academy of Sciences of the United States of America*, vol. 84, no. 23, pp. 8463–8467, 1987.

[5] M. W. Miller, D. L. Miller, and A. A. Brayman, "A review of in vitro bioeffects of inertial ultrasonic cavitation from a

mechanistic perspective," *Ultrasound in Medicine and Biology*, vol. 22, no. 9, pp. 1131–1154, 1996.

[6] M. Joersbo and J. Brunstedt, "Protein synthesis stimulated in sonicated sugar beet cells and protoplasts," *Ultrasound in Medicine and Biology*, vol. 16, no. 7, pp. 719–724, 1990.

[7] W. J. Greenleaf, M. E. Bolander, G. Sarkar, M. B. Goldring, and J. F. Greenleaf, "Artificial cavitation nuclei significantly enhance acoustically induced cell transfection," *Ultrasound in Medicine and Biology*, vol. 24, no. 4, pp. 587–595, 1998.

[8] P. Schratzberger, J. G. Krainin, G. Schratzberger et al., "Transcutaneous ultrasound augments naked DNA transfection of skeletal muscle," *Molecular Therapy*, vol. 6, no. 5, pp. 576–583, 2002.

[9] M. Duvshani-Eshet and M. Machluf, "Therapeutic ultrasound optimization for gene delivery: a key factor achieving nuclear DNA localization," *Journal of Controlled Release*, vol. 108, no. 2-3, pp. 513–528, 2005.

[10] M. Duvshani-Eshet and M. Machluf, "Therapeutic ultrasound optimization for gene delivery: a key factor achieving nuclear DNA localization," *Journal of Controlled Release*, vol. 108, no. 2-3, pp. 513–528, 2005.

[11] H. J. Kim, J. F. Greenleaf, R. R. Kinnick, J. T. Bronk, and M. E. Bolander, "Ultrasound-mediated transfection of mammalian cells," *Human Gene Therapy*, vol. 7, no. 11, pp. 1339–1346, 1996.

[12] Y. Taniyama, K. Tachibana, K. Hiraoka et al., "Development of safe and efficient novel nonviral gene transfer using ultrasound: enhancement of transfection efficiency of naked plasmid DNA in skeletal muscle," *Gene Therapy*, vol. 9, no. 6, pp. 372–380, 2002.

[13] Y. Taniyama, K. Tachibana, K. Hiraoka et al., "Local delivery of plasmid DNA into rat carotid artery using ultrasound," *Circulation*, vol. 105, no. 10, pp. 1233–1239, 2002.

[14] T. Li, K. Tachibana, M. Kuroki, and M. Kuroki, "Gene transfer with echo-enhanced contrast agents: comparison between albunex, optison, and levovist in mice—initial results," *Radiology*, vol. 229, no. 2, pp. 423–428, 2003.

[15] E. C. Unger, T. Porter, W. Culp, R. Labell, T. Matsunaga, and R. Zutshi, "Therapeutic applications of lipid-coated microbubbles," *Advanced Drug Delivery Reviews*, vol. 56, no. 9, pp. 1291–1314, 2004.

[16] S. Sonoda, K. Tachibana, E. Uchino et al., "Gene transfer to corneal epithelium and keratocytes mediated by ultrasound with microbubbles," *Investigative Ophthalmology and Visual Science*, vol. 47, no. 2, pp. 558–564, 2006.

[17] G. Blume and G. Cevc, "Liposomes for the sustained drug release in vivo," *Biochimica et Biophysica Acta*, vol. 1029, no. 1, pp. 91–97, 1990.

[18] T. M. Allen, C. Hansen, F. Martin, C. Redemann, and A. F. Yau-Young, "Liposomes containing synthetic lipid derivatives of poly(ethylene glycol) show prolonged circulation half-lives in vivo," *Biochimica et Biophysica Acta*, vol. 1066, no. 1, pp. 29–36, 1991.

[19] K. Maruyama, T. Yuda, A. Okamoto, S. Kojima, A. Suginaka, and M. Iwatsuru, "Prolonged circulation time in vivo of large unilamellar liposomes composed of distearoyl phosphatidylcholine and cholesterol containing amphipathic poly(ethylene glycol)," *Biochimica et Biophysica Acta*, vol. 1128, no. 1, pp. 44–49, 1992.

[20] K. Maruyama, O. Ishida, S. Kasaoka et al., "Intracellular targeting of sodium mercaptoundecahydrododecaborate (BSH) to solid tumors by transferrin-PEG liposomes, for boron neutron-capture therapy (BNCT)," *Journal of Controlled Release*, vol. 98, no. 2, pp. 195–207, 2004.

[21] Y. Negishi, D. Omata, H. Iijima et al., "Preparation and characterization of laminin-derived peptide AG73-coated liposomes as a selective gene delivery tool," *Biological and Pharmaceutical Bulletin*, vol. 33, no. 10, pp. 1766–1769, 2010.

[22] R. Suzuki, T. Takizawa, Y. Negishi et al., "Gene delivery by combinationof novel liposomal bubbles with perfluoropropane and ultrasound," *Journal of Controlled Release*, vol. 117, no. 1, pp. 130–136, 2007.

[23] R. Suzuki, T. Takizawa, Y. Negishi et al., "Tumor specific ultrasound enhanced gene transfer in vivo with novel liposomal bubbles," *Journal of Controlled Release*, vol. 125, no. 2, pp. 137–144, 2008.

[24] R. Suzuki, T. Takizawa, Y. Negishi, N. Utoguchi, and K. Maruyama, "Effective gene delivery with novel liposomal bubbles and ultrasonic destruction technology," *International Journal of Pharmaceutics*, vol. 354, no. 1-2, pp. 49–55, 2008.

[25] Y. Negishi, Y. Endo, T. Fukuyama et al., "Delivery of siRNA into the cytoplasm by liposomal bubbles and ultrasound," *Journal of Controlled Release*, vol. 132, no. 2, pp. 124–130, 2008.

[26] Y. Negishi, D. Omata, H. Iijima et al., "Enhanced laminin-derived peptide AG73-mediated liposomal gene transfer by bubble liposomes and ultrasound," *Molecular Pharmaceutics*, vol. 7, no. 1, pp. 217–226, 2010.

[27] R. Suzuki, E. Namai, Y. Oda et al., "Cancer gene therapy by IL-12 gene delivery using liposomal bubbles and tumoral ultrasound exposure," *Journal of Controlled Release*, vol. 142, no. 2, pp. 245–250, 2010.

[28] J. C. Fernandes, J. Martel-Pelletier, and J. P. Pelletier, "The role of cytokines in osteoarthritis pathophysiology," *Biorheology*, vol. 39, no. 1-2, pp. 237–246, 2002.

Biomaterials 32 (2011) 5498–5504

Contents lists available at ScienceDirect

Biomaterials

journal homepage: www.elsevier.com/locate/biomaterials

Fine tuning of receptor-selectivity for tumor necrosis factor-α using a phage display system with one-step competitive panning

Yasuhiro Abe [a], Tomoaki Yoshikawa [a,b], Masaki Inoue [a], Tetsuya Nomura [a], Takeshi Furuya [a,b], Takuya Yamashita [a,b], Kazuya Nagano [a], Hiromi Nabeshi [a,b], Yasuo Yoshioka [a,c], Yohei Mukai [a,b], Shinsaku Nakagawa [b,c], Haruhiko Kamada [a,c], Yasuo Tsutsumi [a,b,c], Shin-ichi Tsunoda [a,b,c,*]

[a] Laboratory of Biopharmaceutical Research, National Institute of Biomedical Innovation, 7-6-8 Saito-Asagi, Ibaraki, Osaka 567-0085, Japan
[b] Graduate School of Pharmaceutical Sciences, Osaka University, 1-6 Yamadaoka, Suita, Osaka 565-0871, Japan
[c] The Center of Advanced Medical Engineering and informatics, Osaka University, 1-6 Yamadaoka, Suita, Osaka 565-0871, Japan

ARTICLE INFO

Article history:
Received 24 March 2011
Accepted 5 April 2011
Available online 5 May 2011

Keywords:
Cytokine
Molecular biology
Protein
Affinity
Bioactivity

ABSTRACT

Tumor necrosis factor-α (TNF) is one of the attractive targets for the development of anti-inflammatory and anti-tumor drugs, because it is an important mediator in the pathogenesis of several inflammatory diseases and tumor progression. Thus, there is an increasing need to understand the TNF receptor (TNFR1 and TNFR2) biology for the development of TNFR-selective drugs. Nonetheless, the role of TNFRs, especially that of TNFR2, remains poorly understood. Here, using a unique competitive panning, we optimized our phage display-based screening technique for isolating receptor-selective TNF mutants, and identified several TNFR2-specific TNF mutants with high TNFR2 affinity and full bioactivity via TNFR2. Among these mutants, the R2-7 clone revealed very high TNFR2-selectivity (1.8×10^5 fold higher than that for the wild-type TNF), which is so far highest among the reported TNFR2-selective TNF mutants. Because of its high TNFR2-selectivity and full bioactivity, the TNF mutant R2-7 would not only help in elucidating the functional role of TNFR2 but would also help in understanding the structure-function relationship of TNF/TNFR2. In summary, our one-step competitive panning system is a simple, useful and effective technology for isolating receptor-selective mutant proteins.

1. Introduction

Tumor necrosis factor-α (TNF) is a major inflammatory cytokine that plays a central role in host defense and inflammation via two receptor subtypes, TNF receptor (TNFR)1 and TNFR2 [1,2]. Elevated serum levels of TNF correlates with the severity and progression of the inflammatory diseases such as rheumatoid arthritis (RA), inflammatory bowel disease, septic shock, multiple sclerosis and hepatitis [3–5]. Currently, TNF-neutralization therapies have proven successful for the treatment of RA [4,6,7]. However, these therapies can cause serious side effects, such as tuberculosis, because TNF-dependent host defense functions are also inhibited [8,9]. Therefore, understanding the function of TNF/TNFRs is important for optimal therapy of various TNF-related autoimmune diseases. TNFR1 is constitutively expressed in most tissues and seems to be the key mediator of TNF signaling [10,11]. In contrast, the expression of TNFR2 is more restricted and is found mainly on certain T-cell subpopulations [12], endothelial cells, cardiac myocytes [13] and neuronal tissue [14,15]. Recent studies suggested that TNFR2 signaling is associated with T-cell survival [16], cardioprotection [17,18], remyelination [19], and survival of some neuron subtypes [20,21]. Although the two TNFRs have been shown to have distinct functions in some cells [22], the physiological significance of the presence of both receptors is not fully understood. Especially TNFR2-induced signaling remains elusive and need further investigation.

In order to understand the mechanism of TNFRs, we have investigated the relationship between the biological activities and structural properties of a large number of TNF mutants by phage-display technique [23,24]. However, screening efficiency of isolating TNFR2-selective TNF mutants using this technique is extremely low, and it is difficult to prepare large repertoire of TNFR2-selective TNF mutants for the structure-activity relationship study. In our previous study, we screened 500 phage clones

* Corresponding author. Laboratory of Biopharmaceutical Research, National Institute of Biomedical Innovation, 7-6-8 Saito-Asagi, Ibaraki, Osaka 567-0085, Japan. Tel.: +81 72 641 9814; fax: +81 72 6419817.
E-mail address: tsunoda@nibio.go.jp (S.-i. Tsunoda).

0142-9612/$ – see front matter © 2011 Elsevier Ltd. All rights reserved.
doi:10.1016/j.biomaterials.2011.04.018

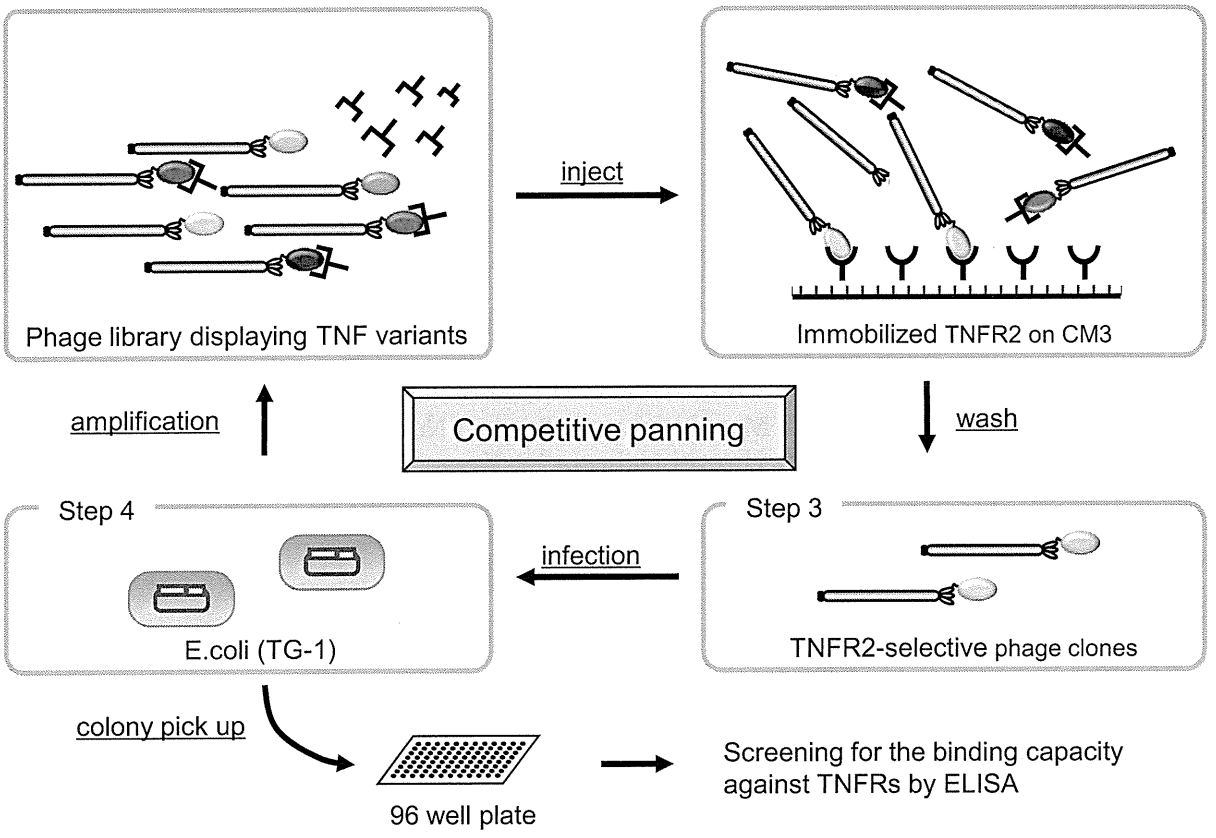

Fig. 1. Screening scheme for isolating TNFR2-selective TNF mutants using competitive panning. To concentrate TNFR2-selective mutant TNFs, phage libraries were pre-incubated with TNFR1 Fc chimera (TNFR1-Fc), and subsequent biopanning against the TNFR2 was carried out in the presence of TNFR1-Fc using the BIAcore biosensor. After several rounds of panning, phage clones were isolated and screened by ELISA.

for isolating TNFR2-selective mutants using the conventional panning method [23]. Out of the 500 clones, only 2 clones showed selectivity for TNFR2 binding that was 10-times higher than the wild-type TNF (wtTNF). Furthermore, bioactivities of these two TNFR2 selective TNF mutants were lower than that of wtTNF (<30%). To improve the screening efficacy, we optimized our phage display-based cytokine mutagenesis technology [25] with an unique competitive panning technique for identifying TNFR2-specific TNF mutants with higher affinity and bioactivity. In this competitive panning technique, phage libraries were pre-incubated with TNFR1 Fc chimera (TNFR1-Fc), and subsequent biopanning against the TNFR2 was carried out in the presence of TNFR1-Fc using the BIAcore biosensor. Since TNFR1-binding clones could not bind to TNFR2 due to steric hindrance, TNF mutants binding only to TNFR2 were selectively enriched with high efficiency. Using this optimized competitive panning technique, we have identified TNFR2-selective TNF mutants with full bioactivity via TNFR2.

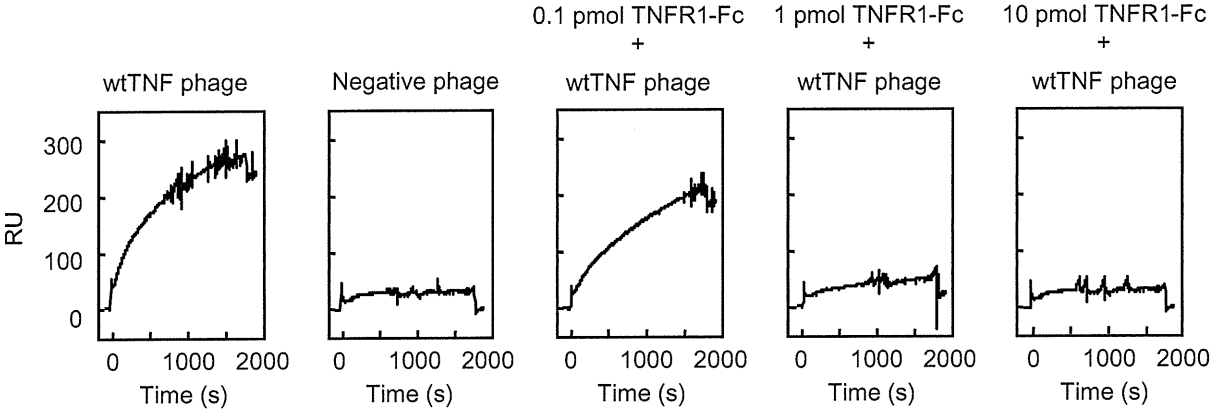

Fig. 2. Optimization of competitive panning using BIAcore biosensor. 0.1 pmol, 1 pmol or 10 pmol of human TNFR1-Fc was mixed with 1×10^{10} CFU phages displaying wtTNF for 2 h at 4 °C, and the mixture was passed over the TNFR2-immobilized CM3 sensor chip and real-time biomolecular interaction analyses were performed with BIAcore biosensor. Anti-CD25 single chain Fv-displaying phage was used as a negative control.

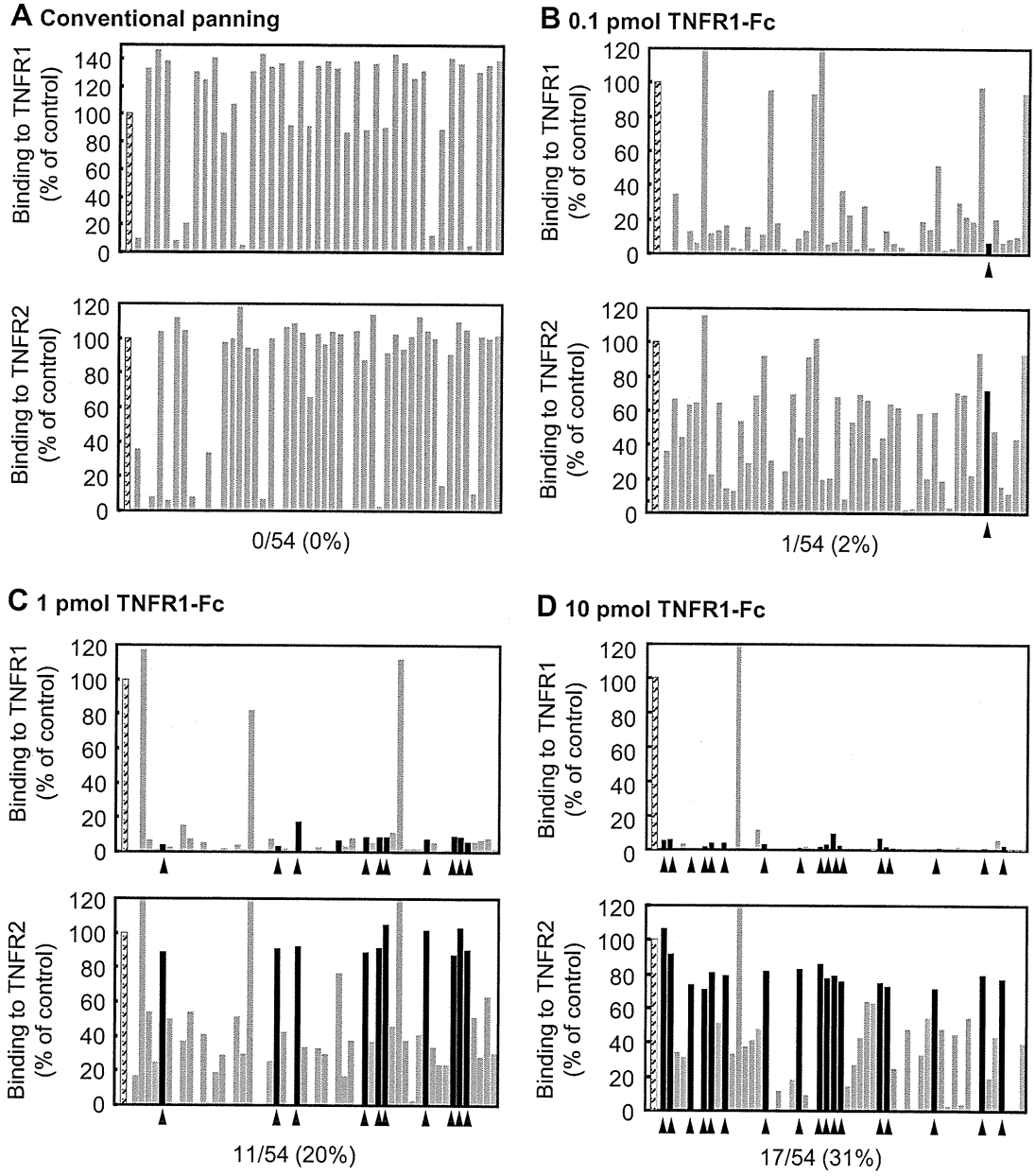

Fig. 3. Determination of relative affinities of mutant TNFs for TNFR1 or TNFR2 by capture ELISA. *E. coli* supernatant containing a TNF mutant (gray bar) from each panning conditions, in which phages were premixed with (A) none, (B) 0.1 pmol, (C) 1 pmol and (D) 10 pmol of TNFR1-Fc, were applied to the TNFR1-Fc or TNFR2-Fc immobilized plate and detected with biotinylated polyclonal anti-TNF antibody. wtTNF was used as a positive control (hatched bar). Affinities of TNFR2-selective clones (black bar) for TNFR2 was more than 70% of that of the wtTNF, and that for TNFR1 was less than 30% of that of the wtTNF.

2. Materials and methods

2.1. Cells

HEp-2 cells, a human fibroblast cell line, were provided by Cell Resource Center for Biomedical Research (Tohoku University, Sendai, Japan) and were maintained in RPMI 1640 (Sigma–Aldrich Japan, Tokyo, Japan) supplemented with 10% bovine fetal serum (FBS) 1 mM sodium pyruvate, 50 mM 2-mercaptoethanol, and antibiotics. hTNFR2/mFas-PA cells are preadipocytes derived from TNFR1$^{-/-}$R2$^{-/-}$ mice expressing a chimeric receptor, the extracellular and transmembrane domain of human TNFR2, and intracellular domain of mouse Fas; these cells were cultured in RPMI 1640 supplemented with 10% FBS, 5 μg/ml Blasticidin S HCl (Invitrogen, Carlsbad, CA), and antibiotics [26].

2.2. Library construction

Protocol for the construction of phage-display library displaying structural mutants of human TNF has been described previously [23]. In brief, multiple-mutations were introduced into the wtTNF gene by PCR to randomly replace the codons of 6 amino acid residues at positions 29, 31, 32, 145, 146 and 147, respectively, of the TNF protein. The PCR product was digested with the restriction enzymes Hind III and Not I, and ligated into the Hind III/Not I digested pY03′ phagemid vector for displaying the TNF mutants on the phage surface as g3p-fusion proteins.

2.3. Optimization of competitive panning using BIAcore biosensor

Human TNFR2-Fc (R&D systems, Minneapolis, MN) was diluted to 50 μg/ml in 10 mM sodium acetate buffer (pH 4.5) and immobilized onto a CM3 sensor chip using an amine coupling kit (GE Healthcare, UK), which resulted in an increase of 5000–6000 resonance units (RU). 0.1 pmol, 1 pmol or 10 pmol of human TNFR1-Fc (R&D systems) was mixed with 100 μl of wtTNF-displaying phage (1×10^{11} CFU/ml) for 2 h at 4 °C, and the mixture was passed over the TNFR2-immobilized CM3 sensor chip at a flow rate of 3 μl/min. The binding kinetics of the mixtures to TNFR2-Fc were analyzed by BIAcore 2000 (GE Healthcare).

Table 1
Amino acid sequences of wtTNF and TNFR2-selective TNF mutants.

Clone	Residue position					
	29	31	32	145	146	147
wtTNF	L	R	R	A	E	S
R2–6	L	R	R	H	E	D
R2–7	V	R	R	D	D	D
R2–8	L	R	R	N	D	D
R2–9	L	R	R	T	S	D
R2–10	L	R	R	Q	D	D
R2–11	L	R	R	T	D	D
R2–12	L	R	R	D	G	D
R2–13	L	R	R	D	E	D

2.4. Selection of phage displaying TNFR2-selective TNF mutants by competitive panning

1×10^{10} CFU phages displaying TNF mutants were pre-incubated for 2 h at 4 °C, with serially diluted TNFR1-Fc. The mixtures were injected at 3 μl/min over the sensor chip. After injection, the sensor chip was washed using the rinse command for 3 min. Elution was carried out using 20 μl of 10 mM glycine-HCl (pH 2.0) and the eluted phage was neutralized with 1 M Tris–HCl (pH 6.9). The recovered phages were amplified by infection of E. coli strain TG1 (Stratagene, La Jolla, CA), which allow read-through of the amber stop codon located between the TNF and g3p sequences of pY03′ phagemid vector. These steps were repeated twice. After final round of panning, the phage mixture was used to infect E. coli and plated on LB agar/ampicillin plates. Single clones of transfected TG1 were randomly picked from the plate and each colony was grown in 2-YT medium with ampicillin (100 μg/ml) and glucose (2% w/v) at 37 °C until the OD_{600} of the culture medium reached 0.4. Each culture was centrifuged, the supernatants were removed, and fresh 2-YT media with ampicillin (100 μg/ml) was added to each E. coli pellet. After incubation for 6 h at 37 °C supernatants were collected and used to determine affinity for TNFRs by capture ELISA as described previously [24]. After the procedure, the phagemid vectors were sequenced using a Big Dye Terminator v3.1 kit and ABI PRISM 3100 (Applied Biosystems Ltd., Pleasanton, CA).

2.5. Expression and purification of TNF mutants

Preparation of purified recombinant protein was described previously [25]. In brief, TNF mutants recombined into pYas1 vector, under the control of T7 promoter, were produced in E. coli (BL21λDE3). Mutant TNFs recovered from inclusion body, which were washed in Triton X-100 and solubilized in 6 M guanidine-HCl, 0.1 M Tris–HCl, pH 8.0, and 2 mM EDTA. Solubilized protein was adjusted to 10 mg/ml and was reduced with 10 mg/ml dithioerythritol for 4 h at RT and refolded by 100-fold dilution in a refolding buffer (100 mM Tris–HCl, 2 mM EDTA, 1 M arginine, and oxidized glutathione (551 mg/L)). After dialysis with 20 mM Tris–HCl, pH 7.4, containing 100 mM urea, active trimeric proteins were purified by Q-Sepharose (GE Healthcare)chromatography and size-exclusion chromatography (Superose 12; GE Healthcare).

2.6. Analysis of binding kinetics using surface plasmon resonance (SPR)

The binding kinetics of the wtTNF and TNF mutants were analyzed by the SPR technique (BIAcore 2000; GE Healthcare). TNFR1-Fc or TNFR2-Fc were separately immobilized on to CM5 sensor chip, resulting in an increase of 3000–3500 RU. During the association phase, wtTNF or TNF mutants diluted in running buffer (HBS-EP) at 156.8, 52.3, 17.4, 5.8 or 1.9 nM were passed over the immobilized TNFR2 for 2 min at a flow rate of 20 μl/min. During the dissociation phase, HBS-EP was run over the sensor chip for 1 min at a flow rate of 20 μl/min. The SPR measurements for TNFR1 were performed using much higher concentrations of TNF mutants (392.1, 130.7, 43.6, 14.5 or 4.8 nM). The data were analyzed globally with BIAevaluation 3.1 software (GE Healthcare) to apply a 1:1 Langmuir binding model. The obtained sensorgrams were fitted globally over the range of injected concentrations and simultaneously over the association and dissociation phages.

2.7. In vitro assessment of bioactivity via TNFR1 or TNFR2 with TNF mutants

HEp-2 cells were seeded at 4×10^4 cells/well in 96-well plates and incubated for 18 h with serially diluted wtTNF (Peprotech, Rocky Hill, NJ) or TNF mutants in the presence of 50 mg/ml cycloheximide. After incubation, cell survival was determined by methylene blue assay as described previously [25]. In the case of analyzing TNFR2-mediated biological activity, hTNFR2/mFas-PA were seeded on 96-well micro titer plates with a density of 1.5×10^4 cells/well in culture medium. Serial dilutions of wtTNF (Peprotech) and TNF mutants were prepared with 1 μg/ml cycloheximide and added to each well. After 48 h-incubation at 37 °C, the cell viabilities were analyzed using a WST-8 assay kit (Nacalai Tesque) according to the manufacturer's instructions.

3. Results

3.1. Optimization of one-step competitive panning protocol

To improve identifying TNFR2-selective TNF mutants with better bioactivity, we have introduced a step to remove the TNFR1-binding phages from the library by competitive panning using TNFR1-Fc. We postulated that TNFR1-binding clones could be eliminated when panning for the TNFR2-binding clones is performed in the presence of TNFR1 protein (see Fig. 1). Although an immunoplate or immunotube is commonly used for the panning [27–29], these techniques cannot make real-time observation of the interaction between phage library and receptor, and are difficult to automate and control the precise settings. Therefore, we first utilized the BIAcore biosensor and optimized the concentration of TNFR1-Fc required for eliminating the TNFR1-binding clones. Serially diluted human TNFR1-Fc was mixed with 1×10^{10} CFU phages displaying wtTNF, and the binding avidity of the phage-displayed wtTNF for TNFR2 was assessed using a BIAcore biosensor. As shown in Fig. 2, TNFR1-Fc inhibited the binding of phage-displayed wtTNF to TNFR2 in a dose-dependent manner. 10 pmol of TNFR1-Fc virtually abolished the binding of wtTNF not only to TNFR2 (last panel in Fig. 2) but also the binding of wtTNF to TNFR1 (data not shown). These results clearly suggest that 10 pmol of TNFR1-Fc would be sufficient for competitively subtract unwanted TNFR1-binding phage clones from a phage library displaying structural TNF mutants.

Table 2
Biding kinetics of TNFs to TNFR1 and TNFR2.

	TNFR1				TNFR2			
	k_{on}[a] (10^6 $M^{-1}s^{-1}$)	k_{off}[b] (10^{-4} s^{-1})	K_D[c] (10^{-10} M)	Relative[d] (%)	k_{on}[a] (10^6 $M^{-1}s^{-1}$)	k_{off}[b] (10^{-4} s^{-1})	K_D[c] (10^{-10} M)	Relative[d] (%)
wtTNF	0.45	1.3	2.9	100.0	2.0	12.1	6.1	100.0
R2–6	0.79	54.5	68.8	4.2	3.2	7.8	2.4	251.4
R2–7	0.44	116.0	262.0	1.1	2.1	7.4	3.6	169.7
R2–8	1.22	50.3	41.1	7.1	3.1	6.6	2.1	291.0
R2–9	1.19	50.1	42.3	6.9	3.8	12.6	3.3	185.2
R2–10	0.67	43.9	63.7	4.6	2.2	5.3	2.4	253.5
R2–11	0.81	87.5	108.	2.7	2.3	5.4	2.3	264.5
R2–12	1.36	98.8	72.6	4.0	4.1	10.6	2.6	235.0
R2–13	0.97	104.0	107.0	2.7	2.9	8.2	2.9	212.2

Kinetic parameters for each TNF were calculated from the respective sensorgram by BIAevaluation 3.1software, and taking into consideration that the TNF binds as a trimer.
[a] k_{on} is the association kinetic constant.
[b] k_{off} is the dissociation kinetic constant.
[c] K_D is the equilibrium dissociation constant ($K_D = k_{off}/k_{on}$).
[d] Relative values were calculated from the K_D (wtTNF)/K_D (TNF mutants) × 100.

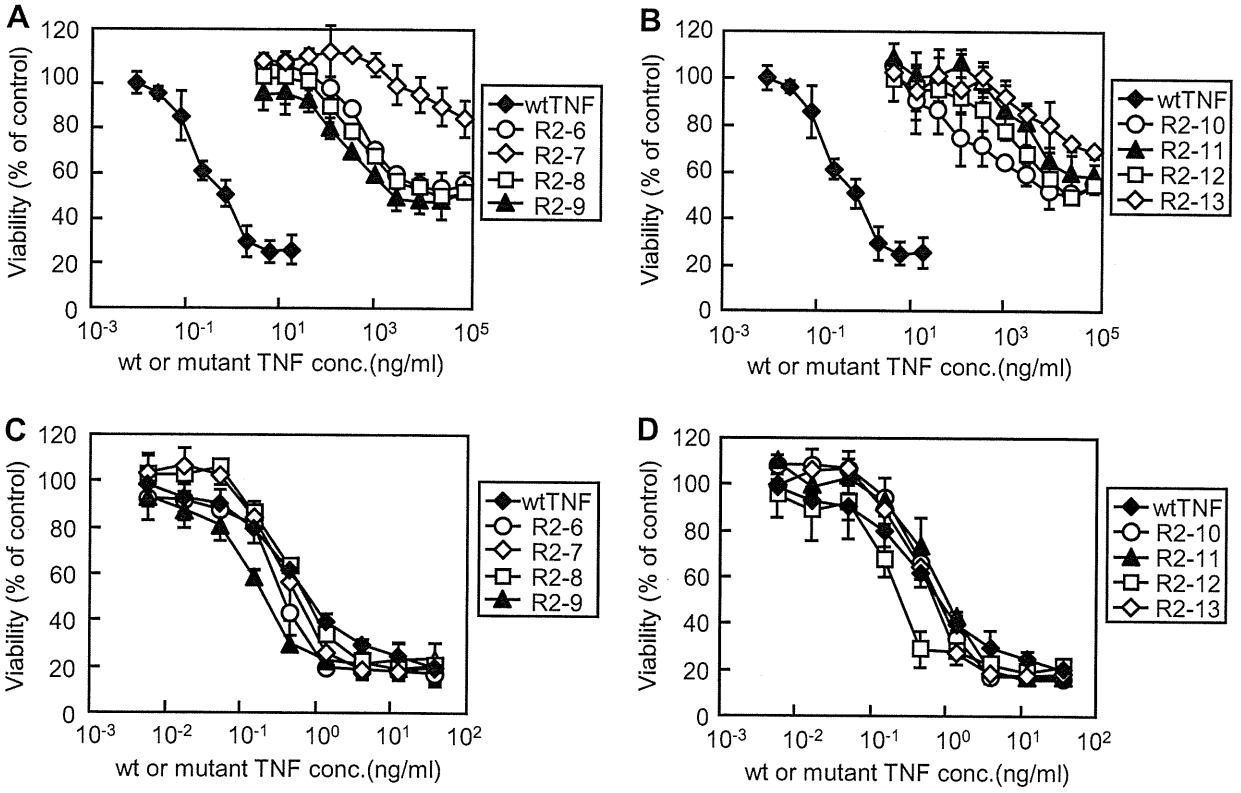

Fig. 4. In vitro bioactivity assay of TNF mutants via TNFR1 or TNFR2. The bioactivity of mutant TNFs via TNFR1 or TNFR2 were measured by cytotoxicity assay against HEp-2 cells (A and B) or hTNFR2/mFas-PA (C and D), respectively. Each point represents the mean ± S.D. of triplicate measurements.

3.2. Selection of TNFR2-selective TNF mutants by one-step competitive panning

To concentrate TNFR2-selective mutant TNFs, the TNF structural mutant displaying phage library was subjected to two rounds of conventional panning or competitive panning against TNFR2 using the BIAcore biosensor. After the second round of panning, *Escherichia coli* (TG1) supernatants of 54 randomly picked clones from each panning procedure were further screened by capture ELISA to analyze their binding specificities for each TNFR (Fig. 3). Consequently, we obtained numerous clones with high-affinity for TNFR2 under all panning conditions. Binding avidities of these clones for TNFR1 tended to decrease depending on the concentration of TNFR1-Fc used for premixing. However, binding avidity of a TNFR2-selective clone, which binds only to TNFR2 (Fig. 3, black bar), tended to increase depending on the concentration of TNFR1-Fc used for premixing. Almost all clones obtained from the conventional and competitive panning with 0.1 pmol of TNFR1-Fc (Fig. 3A and B, respectively) bound to TNFR1, and the panning efficiency for isolating the TNFR2-selective TNF mutants was <2%. In contrast, clones obtained from the subtracted panning with 1 or 10 pmol of TNFR1-Fc (Fig. 3C and D, respectively) contained many TNFR2-selective TNF mutants (>20%). From these panned clones, we eventually identified eight candidate agonists that selectively and strongly bound to the TNFR2. Amino acid sequences of these eight candidate TNFR2-selective TNF mutants are shown in Table 1. TNFR2-slective mutants were mutated near residue 145 and

Table 3
In vitro bioactivities of TNF mutants via TNFR1 or TNFR2.

	TNFR1[a]		TNFR2[b]		TNFR2/TNFR1[e]
	EC50[c] (ng/ml)	Relative Activity[d] (%)	EC50[c] (ng/ml)	Relative activity[d] (%)	
wtTNF	0.6	100	0.56	100	1.0
R2–6	8.1×10^{3}	7.3×10^{-3}	0.39	144	2.0×10^{4}
R2–7	$>1.0 \times 10^{5}$	$<6.0 \times 10^{-4}$	0.51	110	1.8×10^{5}
R2–8	4.6×10^{3}	1.2×10^{-2}	0.67	84	7.0×10^{3}
R2–9	2.1×10^{3}	2.8×10^{-2}	0.21	267	9.5×10^{3}
R2–10	1.1×10^{4}	5.4×10^{-3}	0.72	78	1.4×10^{4}
R2–11	6.7×10^{4}	8.9×10^{-4}	0.95	59	6.6×10^{4}
R2–12	2.6×10^{4}	2.2×10^{-3}	0.23	243	1.1×10^{5}
R2–13	$>1.0 \times 10^{5}$	$<6.0 \times 10^{-4}$	0.63	89	1.5×10^{5}

[a] Bioactivities of the wtTNF and TNF mutants via TNFR1 were measured by determining the TNF-induced cytotoxicity in HEp-2 cells.
[b] Bioactivities of the wtTNF and TNF mutants via TNFR2 were measured by determining the TNF-induced cytotoxicity in hTNFR2/mFas-PA.
[c] Experimental data were analyzed by a logistic regression model to calculate the mean effective concentration (EC50).
[d] Relative activities were calculated from the EC50 (wtTNF)/EC50 (TNF mutants).
[e] Selectivity for TNFR2 was calculated from the ratio of the relative activity (via TNFR2)/relative activity (via TNFR1).

conserved near residue 30. These findings indicate that the amino acid residues near position 30 are an essential for TNFR2 binding.

3.3. Binding kinetics of TNFR2-selective TNF mutants

To investigate the properties of eight TNFR2-selective TNF mutants in detail, we prepared recombinant protein using the previously described methods [30,31]. TNF mutants expressed as an inclusion body in *E. coli* (BL21λDE3) were denatured and refolded. Then, active TNF mutants were purified by ion–exchange and gel–filtration chromatography. TNF mutant purity was greater than 90% in sodium dodecyl sulfate–polyacrylamide gel electrophoresis, and all mutants were confirmed to form homotrimers in the same manner as the wtTNF by gel-filtration analysis (data not shown). To analyze the binding properties of these TNFR2-selective TNF mutants, we determined their binding dissociation constants (kinetic on- and off-rates) for TNFR1 and TNFR2, respectively, in detail using the surface plasmon resonance technique (Table 2). Our analysis showed that all eight mutant TNFs bound to the TNFR2 with high affinity; in contrast, they bound to the TNFR1 with greatly reduced affinity (typically between 1 and 7% of the wtTNF affinity). The dissociation constants (K_D) of these mutants for TNFR2 were between 2.1–3.6 $\times$ 10^{-10} M, and their relative affinities for TNFR2 were between 169 and 291% of that of the wtTNF. Thus, using the competitive panning technique we successfully obtained a large repertoire of TNFR2-selective TNF mutants with different binding parameters (on- and off-rates and dissociation constants).

3.4. Bioactivities of TNFR2-selective TNF mutants

To examine the bioactivity of these TNF mutants via TNFR1, we subsequently performed a cytotoxicity assay using HEp-2 cells (Fig. 4A and B). All TNF mutants (R2-6 ~ R2-13) showed almost no cytotoxicity, and the bioactivity was much lower than that of the wtTNF. Next, we evaluated the TNFR2-mediated activity of TNF mutants using the hTNFR2/mFas-PA, which were previously constructed in our laboratory [26]. The TNFR2-mediated bioactivities of these 8 mutant TNF proteins were at least same or higher than that of the wtTNF (Fig. 4C and D). As a negative control, we determined TNF cytotoxicity in parental $TNFR1^{-/-}R2^{-/-}$ preadipocytes and observed no wtTNF- or mutant TNF-mediated cell death (data not shown). Results of the cytotoxicity assay are summarized in Table 3. R2-7, the most highly TNFR2-selective mutant, exhibited 1.8 $\times$ 10^5 fold higher TNFR2-selectivity than that for the wild-type TNF.

4. Discussion

Recently, it was revealed that the two TNFRs worked together by crosstalk signaling, which suggested that the TNF-mediated signaling in the presence of both TNF receptors actually correlates with their physiological functions [32–34]. To understand the mechanism as well as to analyze the structure–function relationship of the TNFRs, several attempts were made in the past to create TNFR-specific mutant TNFs by conventional site-directed mutagenesis methods (such as Kunkel's method) [35–37]. However, these attempts were not very successful in yielding a desired TNF mutant having high receptor specificity and full bioactivity. For example, the TNFR2-binding affinity of the double mutant D143N-A145R was about 5–10 fold less than the wtTNF [38]. To overcome these problems, we applied phage-display technique and optimized panning method using the BIAcore biosensor (Fig. 1). Using an adequate amount of selective competitive inhibitor (>1 pmol TNFR1-Fc), this one-step competitive panning is ten times more efficient for screening TNFR2-selective TNF mutants, suggesting the competitive panning technology described here is a simple and effective screening method for fine-tuning TNF receptor-selectivity (Fig. 3). As a result of screening, we obtained successfully obtained TNFR2-selective TNF mutants with full bioactivity via TNFR2 (Table 3). Because of its high TNFR2-selectivity and full bioactivity, the TNF mutant R2-7 would help in elucidating the functional role of TNFR2.

One advantage of our phage-display-based technique is that it can be used to obtain the sequence information of many mutants [39,40]. It was previously shown by site-specific mutagenesis technique that mutations at positions 29, 31 and 32 (L29S, R31E and R32W) remarkably reduced the TNF's affinity for binding to TNFR2 [35,37,38]. For most of the TNFR2-selective TNF mutants, amino acids at positions 29, 31 and 32 were indeed identical (except for the R2-7 mutant which contained a conserved L to V substitution at position 29) to those of the wtTNF (Table 1), which is consistent with the previously reported idea that these three amino acids play critical roles in maintaining the binding between the TNF and TNFR2. The amino acid sequence at positions 145, 146 and 147 of the TNFR2-selective TNF mutants were, however, very different from those of the wtTNF. For example, the amino acid residue at position 145 of the TNF mutants R2-7, R2-12 and R2-13 contained an Asp residue in place of the Ala residue, and all of them showed high TNFR2 selectivity. Structural analysis and mutagenesis studies suggested that the loop containing the residues 145–147 is involved in the receptor binding [41–43]. Since Asp is a comparatively large residue, we speculated that this substitution could lead to a steric hindrance disrupting the interaction between the TNFR1 and TNFR2-selective mutants, which may be why they are less TNFR1-selective. However, why this replacement would increase the selectivity for TNFR2 is unclear at this moment. Currently, we are working on determining the structure of the TNF/TNFR2 complex by X-ray crystallography [44] so that structure–activity relationship studies could be initiated in the near future. Additionally, this structural information, in combination with bioinformatics technology, will be useful for designing TNFR-selective inhibitors (peptide mimics and chemical compounds).

5. Conclusions

In this study, we optimized our phage display-based screening using a unique competitive panning technique, which is ten times more efficient for screening TNFR2-selective TNF mutants compared to the conventional panning method. As a result of screening, we have succeeded in isolating several TNFR2-specific TNF mutants with high TNFR2 affinity and full bioactivity via TNFR2. Further analysis of the relationship between the structure and bioactivity of the TNF mutants would offer highly valuable and useful information regarding the TNF/TNFR biology. In conclusion, our fine-tuned competitive panning system is a simple and effective technology for isolating receptor-selective mutant proteins.

Acknowledgment

This study was supported in part by Grants-in-Aid for Scientific Research from the Ministry of Education, Culture, Sports, Science and Technology of Japan, and from the Japan Society for the Promotion of Science (JSPS). This study was also supported in part by Health Labour Sciences Research Grants from the Ministry of Health, Labor and Welfare of Japan, and by Health Sciences Research Grants for Research on Publicly Essential Drugs and Medical Devices from the Japan Health Sciences Foundation.

References

[1] Aggarwal BB. Signalling pathways of the TNF superfamily: a double-edged sword. Nat Rev Immunol 2003;3(9):745–56.
[2] Szlosarek PW, Balkwill FR. Tumour necrosis factor alpha: a potential target for the therapy of solid tumours. Lancet Oncol 2003;4(9):565–73.

[3] Aderka D, Engelmann H, Maor Y, Brakebusch C, Wallach D. Stabilization of the bioactivity of tumor necrosis factor by its soluble receptors. J Exp Med 1992; 175(2):323–9.
[4] Feldmann M, Maini RN. Lasker Clinical Medical Research Award. TNF defined as a therapeutic target for rheumatoid arthritis and other autoimmune diseases. Nat Med 2003;9(10):1245–50.
[5] Muto Y, Nouri-Aria KT, Meager A, Alexander GJ, Eddleston AL, Williams R. Enhanced tumour necrosis factor and interleukin-1 in fulminant hepatic failure. Lancet 1988;2(8602):72–4.
[6] Thorbecke GJ, Shah R, Leu CH, Kuruvilla AP, Hardison AM, Palladino MA. Involvement of endogenous tumor necrosis factor alpha and transforming growth factor beta during induction of collagen type II arthritis in mice. Proc Natl Acad Sci U S A 1992;89(16):7375–9.
[7] Williams RO, Feldmann M, Maini RN. Anti-tumor necrosis factor ameliorates joint disease in murine collagen-induced arthritis. Proc Natl Acad Sci U S A 1992;89(20):9784–8.
[8] Gomez-Reino JJ, Carmona L, Valverde VR, Mola EM, Montero MD. Treatment of rheumatoid arthritis with tumor necrosis factor inhibitors may predispose to significant increase in tuberculosis risk: a multicenter active-surveillance report. Arthritis Rheum 2003;48(8):2122–7.
[9] Lubel JS, Testro AG, Angus PW. Hepatitis B virus reactivation following immunosuppressive therapy: guidelines for prevention and management. Intern Med J 2007;37(10):705–12.
[10] Leist M, Gantner F, Jilg S, Wendel A. Activation of the 55 kDa TNF receptor is necessary and sufficient for TNF-induced liver failure, hepatocyte apoptosis, and nitrite release. J Immunol 1995;154(3):1307–16.
[11] Mori L, Iselin S, De Libero G, Lesslauer W. Attenuation of collagen-induced arthritis in 55-kDa TNF receptor type 1 (TNFR1)-IgG1-treated and TNFR1-deficient mice. J Immunol 1996;157(7):3178–82.
[12] Ware CF, Crowe PD, Vanarsdale TL, Andrews JL, Grayson MH, Jerzy R, et al. Tumor necrosis factor (TNF) receptor expression in T lymphocytes. Differential regulation of the type I TNF receptor during activation of resting and effector T cells. J Immunol 1991;147(12):4229–38.
[13] Irwin MW, Mak S, Mann DL, Qu R, Penninger JM, Yan A, et al. Tissue expression and immunolocalization of tumor necrosis factor-alpha in post-infarction dysfunctional myocardium. Circulation 1999;99(11):1492–8.
[14] Dopp JM, Sarafian TA, Spinella FM, Kahn MA, Shau H, de Vellis J. Expression of the p75 TNF receptor is linked to TNF-induced NFkappaB translocation and oxyradical neutralization in glial cells. Neurochem Res 2002;27(11):1535–42.
[15] Yang L, Lindholm K, Konishi Y, Li R, Shen Y. Target depletion of distinct tumor necrosis factor receptor subtypes reveals hippocampal neuron death and survival through different signal transduction pathways. J Neurosci 2002; 22(8):3025–32.
[16] Ban L, Zhang J, Wang L, Kuhtreiber W, Burger D, Faustman DL. Selective death of autoreactive T cells in human diabetes by TNF or TNF receptor 2 agonism. Proc Natl Acad Sci U S A 2008;105(36):13644–9.
[17] Monden Y, Kubota T, Inoue T, Tsutsumi T, Kawano S, Ide T, et al. Tumor necrosis factor-alpha is toxic via receptor 1 and protective via receptor 2 in a murine model of myocardial infarction. Am J Physiol Heart Circ Physiol 2007;293(1):H743–53.
[18] Wang M, Crisostomo PR, Markel TA, Wang Y, Meldrum DR. Mechanisms of sex differences in TNFR2-mediated cardioprotection. Circulation 2008;118(Suppl. 14):S38–45.
[19] Arnett HA, Mason J, Marino M, Suzuki K, Matsushima GK, Ting JP. TNF alpha promotes proliferation of oligodendrocyte progenitors and remyelination. Nat Neurosci 2001;4(11):1116–22.
[20] Faustman D, Davis M. TNF receptor 2 p.thway: drug target for autoimmune diseases. Nat Rev Drug Discov 2010;9(6):482–93.
[21] Fontaine V, Mohand-Said S, Hanoteau N, Fuchs C, Pfizenmaier K, Eisel U. Neurodegenerative and neuroprotective effects of tumor Necrosis factor (TNF) in retinal ischemia: opposite roles of TNF receptor 1 and TNF receptor 2. J Neurosci 2002;22(7). RC216.
[22] MacEwan DJ. TNF receptor subtype signalling: differences and cellular consequences. Cell Signal 2002;14(6):477–92.
[23] Mukai Y, Shibata H, Nakamura T, Yoshioka Y, Abe Y, Nomura T, et al. Structure-function relationship of tumor necrosis factor (TNF) and its receptor interaction based on 3D structural analysis of a fully active TNFR1-selective TNF mutant. J Mol Biol 2009;385(4):1221–9.
[24] Shibata H, Yoshioka Y, Ohkawa A, Minowa K, Mukai Y, Abe Y, et al. Creation and X-ray structure analysis of the tumor necrosis factor receptor-1-selective mutant of a tumor necrosis factor-alpha antagonist. J Biol Chem 2008;283(2):998–1007.
[25] Yamamoto Y, Tsutsumi Y, Yoshioka Y, Nishibata T, Kobayashi K, Okamoto T, et al. Site-specific PEGylation of a lysine-deficient TNF-alpha with full bioactivity. Nat Biotechnol 2003;21(5):546–52.
[26] Abe Y, Yoshikawa T, Kamada H, Shibata H, Nomura T, Minowa K, et al. Simple and highly sensitive assay system for TNFR2-mediated soluble- and transmembrane-TNF activity. J Immunol Methods 2008;335(1–2):71–8.
[27] Schwarz M, Rottgen P, Takada Y, Le Gall F, Knackmuss S, Bassler N, et al. Single-chain antibodies for the conformation-specific blockade of activated platelet integrin alphallbbeta3 designed by subtractive selection from naive human phage libraries. Faseb J 2004;18(14):1704–6.
[28] Popkov M, Rader C, Barbas 3rd CF. Isolation of human prostate cancer cell reactive antibodies using phage display technology. J Immunol Methods 2004; 291(1–2):137–51.
[29] Eisenhardt SU, Schwarz M, Bassler N, Peter K. Subtractive single-chain antibody (scFv) phage-display: tailoring phage-display for high specificity against function-specific conformations of cell membrane molecules. Nat Protoc 2007;2(12):3063–73.
[30] Shibata H, Yoshioka Y, Abe Y, Ohkawa A, Nomura T, Minowa K, et al. The treatment of established murine collagen-induced arthritis with a TNFR1-selective antagonistic mutant TNF. Biomaterials 2009;30(34):6638–47.
[31] Shibata H, Yoshioka Y, Ikemizu S, Kobayashi K, Yamamoto Y, Mukai Y, et al. Functionalization of tumor necrosis factor-alpha using phage display technique and PEGylation improves its antitumor therapeutic window. Clin Cancer Res 2004;10(24):8293–300.
[32] Wajant H, Pfizenmaier K, Scheurich P. Tumor necrosis factor signaling. Cell Death Differ 2003;10(1):45–65.
[33] Weiss T, Grell M, Siemienski K, Muhlenbeck F, Durkop H, Pfizenmaier K, et al. TNFR80-dependent enhancement of TNFR60-induced cell death is mediated by TNFR-associated factor 2 and is specific for TNFR60. J Immunol 1998; 161(6):3136–42.
[34] Fotin-Mleczek M, Henkler F, Samel D, Reichwein M, Hausser A, Parmryd I, et al. Apoptotic crosstalk of TNF receptors: TNF-R2-induces depletion of TRAF2 and IAP proteins and accelerates TNF-R1-dependent activation of caspase-8. J Cell Sci 2002;115(Pt. 13):2757–70.
[35] Yamagishi J, Kawashima H, Matsuo N, Ohue M, Yamayoshi M, Fukui T, et al. Mutational analysis of structure–activity relationships in human tumor necrosis factor-alpha. Protein Eng 1990;3(8):713–9.
[36] Barbara JA, Smith WB, Gamble JR, Van Ostade X, Vandenabeele P, Tavernier J, et al. Dissociation of TNF-alpha cytotoxic and proinflammatory activities by p55 receptor- and p75 receptor-selective TNF-alpha mutants. Embo J 1994; 13(4):843–50.
[37] Van Ostade X, Vandenabeele P, Everaerdt B, Loetscher H, Gentz R, Brockhaus M, et al. Human TNF mutants with selective activity on the p55 receptor. Nature 1993;361(6409):266–9.
[38] Loetscher H, Stueber D, Banner D, Mackay F, Lesslauer W. Human tumor necrosis factor alpha (TNF alpha) mutants with exclusive specificity for the 55-kDa or 75-kDa TNF receptors. J Biol Chem 1993;268(35):26350–7.
[39] Abe Y, Nomura T, Yoshioka Y, Kamada H, Tsunoda S, Tsutsumi Y. Anti-inflammatory effects of a Novel TNFR1-selective antagonistic TNF mutant on established murine collagen-induced arthritis. Adv Exp Med Biol 2011;691:493–500.
[40] Yoshioka Y, Watanabe H, Morishige T, Yao X, Ikemizu S, Nagao C, et al. Creation of lysine-deficient mutant lymphotoxin-alpha with receptor selectivity by using a phage display system. Biomaterials 2010;31(7):1935–43.
[41] Eck MJ, Sprang SR. The structure of tumor necrosis factor-alpha at 2.6 A resolution. Implications for receptor binding. J Biol Chem 1989;264(29):17595–605.
[42] Van Ostade X, Tavernier J, Fiers W. Structure–activity studies of human tumour necrosis factors. Protein Eng 1994;7(1):5–22.
[43] Idriss HT, Naismith JH. TNF alpha and the TNF receptor superfamily: structure-function relationship(s). Microsc Res Tech 2000;50(3):184–95.
[44] Mukai Y, Nakamura T, Yoshikawa M, Yoshioka Y, Tsunoda S, Nakagawa S, et al. Solution of the structure of the TNF-TNFR2 complex. Sci Signal 2010;3(148). ra83.